RMetS
Royal Meteorological Society

Current problems in scattering radiative transfer modelling for data assimilation

Ralf Bennartz[a]* and Tom Greenwald[b]
[a]*Atmospheric and Oceanic Sciences, University of Wisconsin – Madison, USA*
[b]*Cooperative Institute for Meteorological Satellite Studies, University of Wisconsin – Madison, USA*

*Correspondence to: R. Bennartz, University of Wisconsin Madison, Atmospheric and Ocean Sciences, 1225 W. Dayton St., Madison, Wisconsin, 53706, USA. E-mail: bennartz@aos.wisc.edu

This article assesses current issues related to scattering radiative transfer (RT) in data assimilation (DA) and proposes possible ways to solve or mitigate these issues. Emphasis is put not so much on fundamental issues related to RT but on the practical application within a framework of operational numerical weather prediction and DA with their tight constraints on computational efficiency. In particular, three potentially critical open issues are studied: firstly, the trade-off between speed and accuracy in RT schemes for DA. A numerically efficient method is proposed to determine beforehand whether scattering needs to be accounted for. Secondly, the impact of spectrally highly variable gaseous absorption coefficients within a given instrument's bandpass and its implications on scattering RT is studied. Results of this second part are also put in context with uncertainties caused by the lack of knowledge of scattering optical properties. Finally, model errors due to, for example, the assumption of plane-parallel RT are studied. It is argued that errors caused by plane-parallel RT will likely continue to dominate the error budget both in terms of biases and random errors. Copyright © 2011 Royal Meteorological Society

Received 22 November 2010; Revised 15 September 2011; Accepted 22 September 2011; Published online in Wiley Online Library 25 October 2011

Citation: Bennartz R, Greenwald T. 2011. Current problems in scattering radiative transfer modelling for data assimilation. *Q. J. R. Meteorol. Soc.* **137**: 1952–1962. DOI:10.1002/qj.953

1. Introduction

Satellite data have become the major source of observations in current numerical weather prediction (NWP) analysis systems. Radiance assimilation especially has proven to be a powerful tool to incorporate satellite data into the environment of an NWP model (e.g. Andersson *et al.*, 1994; Derber and Wu, 1998). Prerequisites for radiance assimilation are fast and accurate optical property and radiative transfer models, forward and adjoint, that allow a mapping between radiance and model space. The two most widely used models in an operational context are the Radiative Transfer for TIROS Operational Vertical sounder (RTTOV: Saunders *et al.*, 2007) radiative transfer model and the US Joint Center for Satellite Data Assimilation's (JCSDA's) Community Radiative Transfer Model (CRTM: Weng, 2007). RTTOV is jointly developed by various European centres under the auspices of the European Meteorological Satellite system's (EUMETSAT's) Satellite Application Facility on Numerical Weather Prediction (SAF-NWP). Secondly, these models provide the key interfaces between NWP models and satellite observations, allowing simulation of radiances for a large set of satellites and providing data assimilation (DA) schemes with adjoints and tangent-linear radiative transfer (RT) modules used in variational assimilation. Both models have a long heritage beginning in the 1970s and 1980s (e.g. McMillin and Fleming, 1976; Eyre and Woolf, 1988) when assimilation of satellite observations were first exploited and fast and accurate radiative transfer models were needed.

Initially, these models were limited to non-scattering, cloud-free infrared and microwave radiative transfer. With an increased recognition of the importance of DA under cloudy and precipitating conditions (e.g. Errico *et al.*, 2007),

Copyright © 2011 Royal Meteorological Society

these operational models were gradually extended to include RT solvers that account for scattering (Matricardi, 2005; Bauer *et al.*, 2006; Heidinger *et al.*, 2006; Liu QH and Weng, 2006; O'Dell *et al.*, 2006). Ideally, this would allow for the assimilation of observations under all weather conditions, and initial attempts to do so have shown promising results but also highlighted potential issues both on the RT model side and the NWP model side. The RT modelling issues are largely described by speed versus accuracy issues as well as by the representation of gas absorption and particle scattering properties within the RT model (e.g. Kulie *et al.*, 2010). A second issue arises when interpreting deviations between simulated and observed radiances under scattering conditions. Observed clouds and precipitation patterns are generally spatially inhomogeneous and are very difficult for NWP to adequately simulate. Various studies point out large deviations between observed and simulated radiances under cloudy conditions (O'Dell *et al.*, 2007; Chen *et al.*, 2008; Geer *et al.*, 2009). Here, these errors are termed representativeness errors as they arise not so much from RT-modelling uncertainties but more generally from the limitations of models, NWP as well as RT, in representing the three-dimensional structure of clouds and precipitation.

This article discusses both RT model errors as well as the representativeness errors. It does not strive to give an all-encompassing overview on all possible issues related to scattering RT. Rather, it attempts to highlight several issues, weigh their relative importance, and propose possible solutions. The main part of this paper is separated into three sections (sections 2 to 4). The first two deal with the solution of the plane-parallel RT equation under scattering and absorbing conditions, with section 2 also including a comparison between the RTTOV and CRTM. The third section provides a brief summary of issues related to absorption–scattering interactions as relevant to DA. The fourth section deals with the representativeness error. Results are summarized and an outlook is given in the conclusions.

2. Radiative transfer solvers

2.1. The radiative transfer equation (RTE)

The plane-parallel RTE for diffuse radiation can be written as:

$$\mu\frac{\mathrm{d}I}{\mathrm{d}\tau} = \underbrace{-I}_{\text{I:Attenuation}} + \underbrace{(1-\omega_0)B}_{\text{II:Thermal Source}} + \underbrace{\frac{\omega_0}{4\pi}P(\Omega_S,\Omega)S_S\mu_S\mathrm{e}^{-\tau/\mu_S}}_{\text{III:Solar Source}} + \underbrace{\frac{\omega_0}{4\pi}\int_{\Omega'} I(\Omega')P(\Omega',\Omega)\mathrm{d}\Omega'}_{\text{IV:Multiple Scattering}} \quad (1)$$

with all symbols described in appendix A. While the solar source term can in principle be integrated into the multiple scattering term, it is often preferable to treat solar radiation as a source function for diffuse radiation. For different satellite sensors, this equation can be significantly simplified. The solar source term (III) can be ignored in the microwave and infrared spectral range, whereas the thermal source term (II) can be ignored in most of the solar spectral range. Only in the overlap regions between the solar and terrestrial spectrum at roughly 3–5 μm do both terms need to be considered. However, even in the overlap region the thermal (I+II+IV) and solar RT (I+III+IV) can be decoupled. If atmospheric polarization is to be considered as well, all occurrences of I, S_S and B are to be replaced by their corresponding Stokes vectors, and the phase function P becomes the phase matrix.

A significant simplification arises when scattering can be ignored altogether, in which case terms (III) and (IV) in Eq. (1) can be ignored. In this case the RTE can be integrated formally, yielding Schwarzschild's equation. This is the case for cloud-free infrared as well as for precipitation-free microwave RT. Note that even for weakly reflecting surfaces, reflection off the surface of both solar and thermal radiation might have to be accounted for even if atmospheric scattering can be neglected. Radiance assimilation schemes heavily rely on integrating Schwarzschild's equation because numerically efficient solutions exist and it can be used in DA under cloud-free conditions.

2.2. Speed versus accuracy in scattering RT

In the presence of multiple scattering the solution of the RTE is mathematically more challenging. However, at infrared and microwave wavelengths, where multiple scattering is much weaker relative to non-absorbing solar wavelengths, a variety of very fast solution methods are available, some more accurate than others (e.g. Kummerow, 1993; Greenwald *et al.*, 2005; Heidinger *et al.*, 2006; Liu QH and Weng, 2006). For data assimilation applications in operational environments, speed and accuracy are the most important factors in choosing a solution method.

The solver used in the most recent version of the CRTM (v2.0.2) is a hybrid approach that combines the matrix operator method (Liu QH and Ruprecht, 1996), which solves analytically for the reflection/transmission properties of a homogeneous layer, and the adding method that solves for radiances at each level of the atmosphere. This one solver is used from solar to microwave wavelengths and allows for fully polarized radiative transfer in the atmosphere.

In contrast, RTTOV v10 uses different solvers at infrared and microwave wavelengths. At infrared wavelengths, RTTOV offers a choice of a simple solution for a black, single-layer cloud and a parametrized solution (based on scaling the cloud scattering properties) for multiple cloud layers (Hocking *et al.*, 2011). This study investigates the latter method. At microwave wavelengths, the well-known delta-Eddington approximation is used through a separate interface called RTTOV-SCATT (Bauer *et al.*, 2006).

To compare the speed of the CRTM and RTTOV solvers, a large collection of profiles (95 703) from European Centre for Medium-range Weather Forecasts (ECMWF) analyses for a wide range of cloud and precipitation conditions over both land and ocean was assembled in order to compute brightness temperatures for the 20-channel High-resolution InfraRed Sounder HIRS-4 (3.76–14.96 μm), 15-channel Advanced Microwave Sounding Unit AMSU-A (23.8–89 GHz), and 5-channel Microwave Humidity Sounder MHS (89–190 GHz). The solar component for the short-wave channels of the HIRS-4 was excluded from this comparison. Calculations were done at a single zenith angle of 0° for each channel of each sensor.

Various assumptions had to be made for both models. Because the ECMWF profiles did not contain information about particle size for the four hydrometeor types in the

Copyright © 2011 Royal Meteorological Society

Table I. Comparison of normalized CPU time (seconds per instrument channel) for the RTTOV v10 and CRTM v2.0.2 for each instrument separated into time spent in the radiative transfer solver and total overall time. For details see text.

	HIRS-4 (s/chan)	AMSU-A (s/chan)	MHS (s/chan)
RTTOV solver	0.755	1.18	1.21
RTTOV total	4.42	4.24	5.44
CRTM 2-strm solver	57.0	55.8	75.7
CRTM 2-strm total	107	132	163
CRTM 4-strm solver	106	91.2	118
CRTM 4-strm total	160	176	215

CRTM (cloud ice, cloud liquid water, snow and rain), particle size was randomly selected from within a range of sizes expected for each particle type. For RTTOV-SCATT, land surface emissivity was assigned a constant value of 0.9. For RTTOV infrared calculations, hexagonally shaped ice crystals and the Wyser parametrization were selected for cloud ice. Since RTTOV limits the number of cloud types at any one layer to two, the category of 'cirrus' was used for cloud ice, whereas liquid water clouds were assumed to be 'continental cumulus polluted' over land and 'maritime cumulus' over ocean. Furthermore, RTTOV does not allow for precipitating clouds at infrared wavelengths; therefore, the CRTM calculations for HIRS-4 excluded precipitation.

Additional steps were taken to ensure that a fair comparison was made with regard to execution time. For example, the same Fortran compiler was used with identical settings (i.e. Intel's ifort v11.1 with −O2 optimization) and the models were run on a single CPU core since RTTOV has parallel-processing capabilities.

The RTTOV solvers are found to be 47× to 75× faster, depending on sensor and solver, than the CRTM solver in 2-stream mode (see Table I). The largest differences are due to the fact that the CRTM rigorously computes multiple scattering, whereas the RTTOV infrared solver does not. However, large differences seen even at microwave wavelengths are somewhat surprising given that earlier tests of the delta-Eddington approximation have shown it to be slightly slower in most cases than successive-order-of-scattering and successive-order-of-interaction methods (Greenwald *et al.*, 2005; O'Dell *et al.*, 2006). These methods have been shown by the authors, who are CRTM developers, to be somewhat slower than the solver used in the current CRTM. It may be that this particular implementation of the delta-Eddington approximation within RTTOV is optimized in some way.

Other noticeable differences are evident in terms of the amount of time each model spends doing other non-solver operations, such as computing gas transmittances, initializing cloud optical properties, etc. Subtracting the solver time from the total time (the total time only considers forward calculations within each model) in Table I shows that RTTOV is still 14× to 25× faster than the CRTM even before the solver is executed. Further comparisons using clear-sky profiles show that RTTOV is 5× to 20× faster than the CRTM, suggesting that much of the difference appears to be related to clear-sky calculations in the respective code.

Testing the accuracy of the solvers is a significant challenge because RTTOV accounts for cloud overlap while the CRTM does not, and because the same optical properties input to the respective solvers would have to be made available as input to another highly accurate solver. Such an undertaking is beyond the scope of this study. However, a summary of the accuracy of the RTTOV solvers will be provided based on past studies, and an internal accuracy test will be done on the CRTM because of its multi-stream capability. It should be emphasized that we are concerned here with the accuracy of the solution to the *monochromatic* RTE. Uncertainties arising from the use of polychromatic effective gas and cloud properties across the instrument bandpass will be discussed later, in section 3.

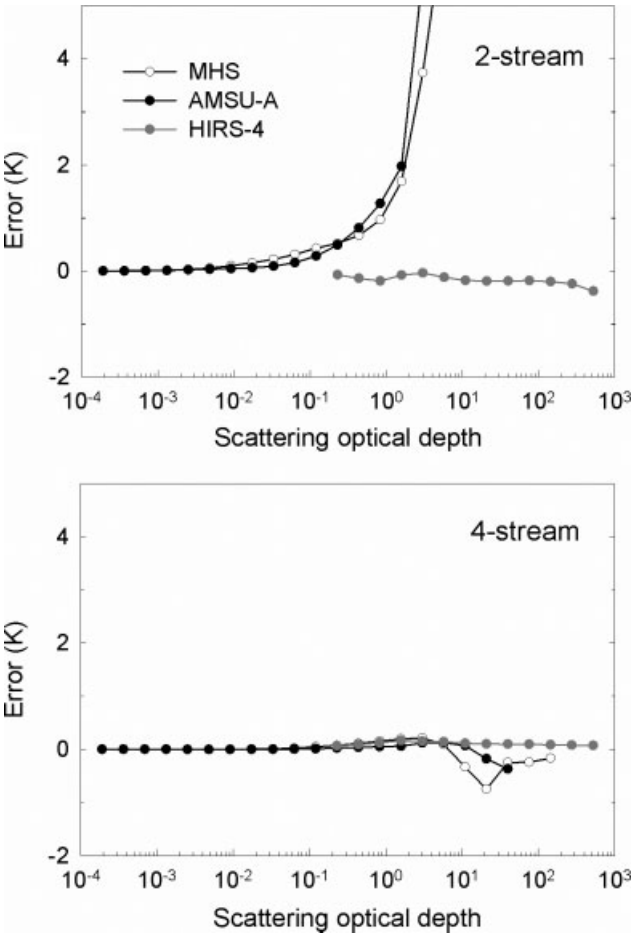

Figure 1. Accuracy of the CRTM 2-stream and 4-stream RT solvers for the same cases/instruments as in Table I plotted against total atmospheric scattering optical depth. Accuracy was evaluated against the 16-stream solver.

The delta-Eddington approximation has been shown to be accurate to within about 2 K over a wide range of microwave wavelengths and precipitation conditions (Kummerow, 1993; Smith *et al.*, 2002; Greenwald *et al.*, 2005; O'Dell *et al.*, 2006), demonstrating its suitability for data assimilation. The accuracy of the RTTOV infrared solver is also below 2 K for marine and continental cumulus at wavelengths greater than about 4.3 μm but well under 0.5 K for cirrus at all infrared wavelengths (Matricardi, 2005).

For the CRTM solver, an accuracy comparison is shown in Figure 1 for 2- and 4-streams (errors averaged for each instrument) as a function of the column scattering optical depth, which in the microwave, at least, is a measure of the degree of scattering. While the 4-stream solution can provide very good accuracy across both the infrared and microwave,

Copyright © 2011 Royal Meteorological Society

it is 1.6 × −1.8× slower than the corresponding 2-stream solution (see Table I); however, there are conditions under which the 2-stream solution is sufficient, which can provide a saving in run-time. It would, therefore, be beneficial to devise a universal way (i.e. applicable for all wavelengths) to automatically determine the optimal number of streams for a given situation. One such way is described in the next section.

2.3. *Assessing the importance of scattering*

When top-of-atmosphere (TOA) radiances are simulated, the importance of scattering in the atmosphere depends on what fraction of the simulated radiances at the TOA has undergone scattering. In strongly absorbing spectral bands, the amount of scattering in the lower atmosphere can be very high but the contribution of scattering at the TOA will essentially be zero due to absorption from the portion of the atmosphere above the scattering layers. The maximum contribution of scattering to the signal at the TOA can be determined from the atmospheric optical properties alone, before invoking potentially time-consuming RT calculations. The following quantity, termed here 'scattering indicator', provides a normalized measure of how much scattering will matter in a scattering and absorbing atmosphere:

$$x_s = \frac{\int_0^{\mathrm{TOA}} \beta_S e^{-\tau_A(z)/\mu} dz}{\int_0^{\mathrm{TOA}} \beta_S dz} \qquad (2)$$

with τ_A being the absorption optical depth between TOA and level z:

$$\tau_A(z) = \int_z^{\mathrm{TOA}} \beta_A dz. \qquad (3)$$

The quantity x_s is normalized so that $0 \leqslant x_S \leqslant 1$ with the two limiting cases:

$x_S \to 0$: No contribution of scattering at TOA

$x_S \to 1$: Only contribution of scattering at TOA

The column-integrated quantity x_S can be interpreted physically as the fraction of scattering optical depths not obstructed by absorption. All optical properties in the integral have to be calculated before the RT is performed, so that x_S can be calculated on the fly with very little computational overhead. For practical purposes, the decision on which RTE solver to use can be made empirically by defining conservative thresholds on x_S.

As an example of how this quantity may be used, x_S and brightness temperatures were calculated (assuming a zenith angle of 0°) from CRTM v2.0.2 for the 8461 channels of the Infrared Atmospheric Sounding Interferometer (IASI) for a single-layer cirrus cloud at 300 hPa with effective particle radius of 30 μm and optical depth of 1.6 (Figure 2). These cloud conditions were chosen to maximize the effects of multiple scattering. As expected, window spectral regions exhibit the highest values of x_S, whereas strong absorption bands have values close to 0. This behaviour is reflected in the 2-stream solution as well, which shows that errors are greatest where x_S is largest and least where it is near 0. If errors are plotted as a function of x_S, a clear separation develops between the 2- and 4-stream errors. It is this separation that allows an x_S threshold to be applied. Although exactly what the threshold should be is somewhat arbitrary, it could be based on the noise level of a given channel. This approach may also be useful for determining whether scattering calculations are even necessary and for selecting other solution methods based on accuracy versus speed trade-offs.

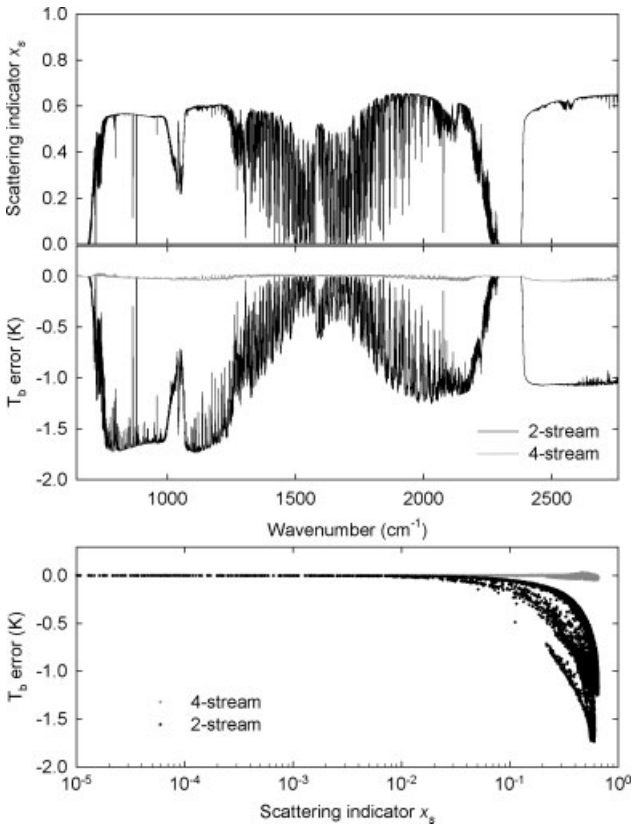

Figure 2. Example of 2-stream and 4-stream errors of a simulated IASI spectrum under scattering conditions. Upper panel shows the scattering indicator defined in Eq. (2) as a function of wave number. The middle panel shows the 2-stream and 4-stream errors (with a 16-stream version of the CRTM solver used as a reference). Lower panel shows errors plotted against the scattering indicator. For details see text.

2.4. *Scattering optical properties*

The practical implementation of scattering RT in a DA context requires the availability of scattering optical properties of atmospheric constituents. Except maybe for the simplest case of pure Rayleigh scattering and the use of anomalous diffraction theory (Greenwald *et al.*, 2002), this requires the tabulation of pre-calculated optical properties for sets of particles. Various methods exist to calculate optical properties for spherical and non-spherical particles. A complete description of scattering optical properties of various particles at different wavelengths is beyond the scope of this paper. Only a few general issues related to scattering optical properties and DA are highlighted here: firstly, given a bulk quantity of scatterers, how does one find the most representative corresponding optical properties given the large number of possible particle habits/size distributions?

Copyright © 2011 Royal Meteorological Society

Secondly, what are the associated uncertainties and how can they be assessed? While this will be briefly discussed by example of microwave scattering of ice particles, note that similar non-spherical databases are available for the infrared as well (e.g. Baum *et al.*, 2005). Various recent publications have theoretically assessed single particle and size-distribution averaged microwave scattering properties of non-spherical particles (Liu GS, 2004; Kim, 2006; Hong, 2007; Matrosov, 2007; Kulie *et al.*, 2010; Petty and Huang, 2010). For practical purposes the validity of the different scattering models will have to be evaluated against multi-spectral observations. One such approach is outlined in Kulie *et al.* (2010) where, within a consistent modelling framework, various scattering models are compared against active and passive microwave observations. This approach allows for the elimination of unrealistic particle models (such as 'soft spheres') as well as for a derivation of observation errors and error covariances induced by the lack of knowledge about, e.g., ice particle habits. Such off-line studies can be used to identify scattering models and associated uncertainties over a wide range of atmospheric conditions, which then can replace older and potentially less well-suited scattering databases in operational models.

Table II provides a brief assessment of errors in scattering calculations caused by uncertainties in scattering optical properties. Calculations were performed for HIRS-3 channels 1–12 using the Successive Order of Interaction radiative transfer model (SOI: Heidinger *et al.*, 2006), High-resolution Transmission molecular absorption (HITRAN) gas optical properties (Rothman *et al.*, 2005), a midlatitude standard atmosphere, and nadir view. A cirrus cloud of optical depth 5 (and 1 km geometrical depth) was placed at 10 km altitude. The single scatter albedo ($0.5 \leqslant \omega_0 \leqslant 0.6$) and asymmetry parameter ($0.85 \leqslant g \leqslant 0.95$) of this cirrus cloud were varied within a reasonable range of uncertainty based on the values provided by Baum *et al.* (2005). The third column in Table II provides the uncertainties in simulated brightness temperatures. The fifth column provides the corresponding scattering indicator value. (Column four of Table II will be discussed subsequently in section 3.)

For channels with high scattering indicator values, the uncertainty in brightness temperatures is on the order of 0.5–2.5 K. For comparison, the last three rows of Table II provide an assessment of brightness temperature uncertainties caused by lack of knowledge of ice habit for three typical microwave window frequencies (from Kulie *et al.*, 2010). The results summarized in Table II only provide a rough indication of the magnitude of expected uncertainties and have to be interpreted with caution. Obviously, these values also vary with observation geometry, cloud height and cloud optical thickness. Note also, that the microwave results are slightly different from the infrared results in methodology as well as in the type of ice particles assessed (precipitation-sized ice for the microwave versus small cirrus crystals for the infrared). A full systematic assessment of errors and error covariances, especially for the infrared, is still an outstanding issue. In the context of this article, in particular with respect to the discussion in section 2.3 and the following discussion in section 3, it is noteworthy that uncertainties caused by lack of knowledge of scattering properties are on the order of a few Kelvin.

3. Accounting for non-monochromatic bandpasses under scattering

The RT equation is strictly valid only monochromatically, whereas remote-sensing instruments observe radiances convolved over a bandpass filter $F(\lambda)$ of the general form:

$$\bar{I}_{\mathrm{OBS}} = \frac{\int I(\lambda)F(\lambda)\mathrm{d}\lambda}{\int F(\lambda)\mathrm{d}\lambda} \tag{4}$$

If gas absorption varies strongly within a satellite bandpass, the averaged transmission will always be higher than the transmission calculated based on the average optical depth. If optical properties were naïvely averaged spectrally and radiative transfer was performed on those averaged optical properties, this would result in large errors. For example, in the monochromatic case, the transmittance through a set of layers equals the product of the transmittances of the individual layers, i.e. monochromatic transmittances are multiplicative. This multiplicative nature of monochromatic transmittances would be violated, if bandpass-averaged optical properties were used in RT calculations.

CRTM and RTTOV currently use similar approaches to account for non-monochromatic bandpasses (McMillin and Fleming, 1976; Fleming and McMillin, 1977; Eyre and Woolf, 1988; Sherlock *et al.*, 2003; Matricardi *et al.*, 2004). In short, an *effective band-averaged transmittance* for each layer is calculated based on a top-down approach as the ratio between the band-averaged transmittance from the TOA down to the base of the layer divided by the band-averaged transmittance from the TOA to the top of the layer. This is done so that the multiplicative nature of transmittances is maintained. When used operationally, this effective optical transmittance (or the corresponding *effective optical depth* taken as minus the logarithm of the effective transmittance) is tabulated for each absorber or predicted by regression based on a set of variables including temperature, absorber amount, zenith angle, and others. Under non-scattering conditions, this approach allows the simulation of each channel with just one RT simulation and results in errors typically lower than the instrument noise. Unlike the physical optical depth of a given layer, however, the effective optical depth will depend on zenith angle because the effect of transmittance above the layer is factored into the calculation of the effective optical depth. Also, regardless of its physical optical depth, the effective optical depth of a layer 'hidden' underneath another optically thick layer will always approach zero, since it will not contribute to the radiation field at the TOA. A corollary of this consideration is that even under non-scattering conditions, in-layer transmittances and heating rate profiles cannot be calculated with such an approach, because hidden layers will have zero effective optical depth.

More elaborate approaches such as Optimal Spectral Sampling (OSS: Moncet *et al.*, 2008), principle component RT (PCRTM: Liu X *et al.*, 2006), or *k*-distribution approaches (e.g. Bennartz and Fischer, 2000) avoid the effective optical depth issue at the cost of subdividing the spectral interval into several spectral intervals that are (optically) similar enough to be treated monochromatically. This is done at the cost of increasing the number of RT simulations needed to simulate a given channel. While this is in general not desirable in DA, if many channels have to

Copyright © 2011 Royal Meteorological Society

Table II. Summary of errors and uncertainties in scattering calculations for HIRS-3 channels 1–12 and selected AMSU and MHS window channels. HIRS calculations were performed for a midlatitude standard atmosphere with a cloud optical thickness of 5 at 10 km altitude. 'Ice model uncertainty' refers to uncertainties in single-scattering albedo of $\omega_0 = 0.55 \pm 0.05$ and in asymmetry parameter of $g = 0.90 \pm 0.05$. The last column gives the maximum absolute error induced by the effective optical depth radiative transfer (see also Figure 3). The last three rows provide error ranges for ice model uncertainties following a different methodology (from Kulie *et al.* (2010), see Tables III and IV therein).

HIRS, AMSU or MHS channel no.	Wave number or frequency	Ice model uncertainty (K)	Absolute error eff. opt. depth (K)	Scattering indicator x_s
HIRS 1	668.9 cm^{-1}	0.02	0.01	0.03
HIRS 2	680.1 cm^{-1}	0.01	0.01	0.09
HIRS 3	691.1 cm^{-1}	0.03	0.12	0.16
HIRS 4	702.8 cm^{-1}	0.12	0.35	0.25
HIRS 5	715.8 cm^{-1}	0.43	0.52	0.33
HIRS 6	731.9 cm^{-1}	0.70	0.54	0.37
HIRS 7	748.1 cm^{-1}	0.99	0.34	0.41
HIRS 8	899.9 cm^{-1}	1.90	0.02	0.43
HIRS 9	1029.1 cm^{-1}	2.10	0.01	0.43
HIRS 10	801.5 cm^{-1}	1.53	0.09	0.43
HIRS 11	1364.9 cm^{-1}	0.92	0.22	0.41
HIRS 12	1527.1 cm^{-1}	0.16	0.28	0.37
AMSU-A 1	23 GHz	1.4–1.7	–	–
AMSU-A 2	89 GHz	2.3–4.0	–	–
MHS 2	157 GHz	2.2–2.3	–	–

be simulated at the same time (e.g. hyperspectral sounders), approaches like OSS or PCRTM will have a significant advantage even in non-scattering cases because a given set of monochromatic RT simulations might allow one to reconstruct the entire spectrum.

The current operational effective optical depths approach has a potentially important limitation in scattering RT: if scattering significantly contributes to the radiation field (terms III and IV in Eq. (1)), the radiation path is not entirely determined by the geometry of the problem anymore. Significant contributions to the TOA radiance might arise from paths shorter (e.g. direct reflection off high clouds) or longer (e.g. multiple scattering) than the geometrical path. For a discussion of this issue in the context of actual photon path lengths, see e.g. Bennartz and Preusker (2006). The key point here is that both shorter and longer paths violate the key assumption made in the calculation of effective optical depths, where the contribution of each layer is weighted solely by its transmission along the direct geometrical path.

Table II, column four, provides the error caused by the effective optical depth approach for the case of a cirrus cloud of optical depth 5 at 10 km altitude (see also section 2.3). Reference results were obtained from high spectral resolution RT simulations, which were convolved according to Eq. (4). Next, the effective optical depth was calculated for the same scene and a single RT simulation was performed using those effective optical depths. Maximum errors induced by the effective optical depth calculation under these conditions are on the order of 0.5 K at HIRS spectral resolution. Note, that HIRS channels 1 and 2 exhibit very small errors, since they peak above the cloud (x_S near zero). Note further, that HIRS channels 7–9 also exhibit small errors even though they see the cloud (x_S near 0.4). In this case the errors are small because the spectral variation in gas optical depth within the bandpass is small (window channels). Most strongly affected are HIRS channels 5–7, which peak near the height of the cirrus cloud *and* exhibit a strong variation of optical depth within the bandpass. For those channels, if scattering is present, the error induced by the effective optical depth approach is larger than the error induced by lack of knowledge of ice scattering optical properties (Table II, value in column 4 larger than value in column 3).

Figure 3 shows for HIRS channel 5 the effective optical depth error for the cloud at 10 km and optical depth 5 but for variable single-scatter albedo and asymmetry parameter. One can see that the error varies depending on the value of g and ω_0. Also the sign of the error varies (note: Table II only lists absolute errors). In general, errors get larger for increasing single-scattering albedo, i.e. if the cloud is scattering more strongly. If the asymmetry parameter is small (less forward scattering, more back-scattering), then the effective optical depth approach is biased warm (negative value in Figure 3).

The smaller box in the top part of the plot highlights the physically realistic range based on Baum *et al.* (2005) as the full range of g and ω_0 given in Figure 3 exceeds the physically realistic range in the infrared. Even within this reduced range, the sign of the error can vary.

Results in Figure 3 pertain to HIRS resolution. However, Figure 4 shows that the issue becomes more severe if the spectral resolution of the sensor is higher, here 0.5 cm^{-1}, a characteristic width for a hyperspectral sounder. The middle plot shows simulated radiances at 0.001 cm^{-1} (cloud 10 km, cloud optical depth 1, $g = 0.85$, $\omega_0 = 0.55$), as well as the same spectra convolved to 0.5 cm^{-1} (red), and corresponding effective optical depth simulations (blue). The spectral region was chosen so that various strong absorption lines as well as more transparent areas are folded within a 0.5 cm^{-1} bandpass. The resulting variability of high-resolution gas absorption optical depth (upper panel) in this region is quite high: The weighting functions of

Copyright © 2011 Royal Meteorological Society

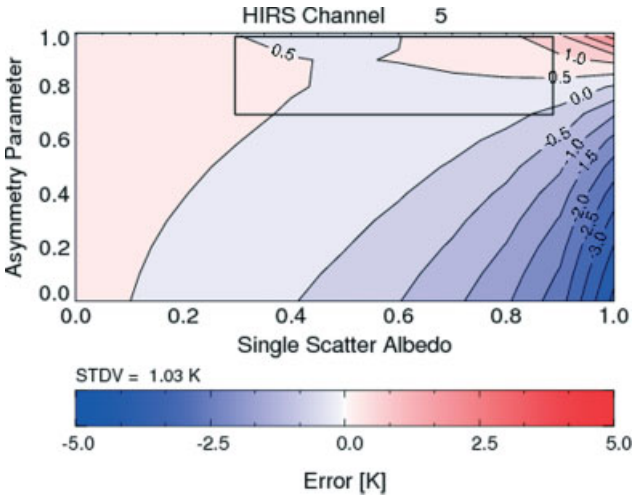

Figure 3. Errors induced by the effective optical depth approach if scattering is present. Simulations were performed for a midlatitude standard atmosphere with a cloud optical thickness of 5 at 10 km altitude. Asymmetry parameter and single-scattering albedo of the cloud were varied beyond their natural range of variability to highlight the systematic behaviour of the errors. The rectangular box in the upper part of the plot gives an indication of the natural variability of ice optical properties based on the Baum *et al.* (2005) ice scattering models. Results are shown for HIRS-3 channel 5. For more details see text.

the line centres peak well above the tropopause, whereas the less absorbing parts of the spectrum peak in the upper troposphere. Resulting errors for the effective optical depth can approach 2 K (differences between the red and blue curve also given in the lower panel).

While the examples above only highlight the issue, some general conclusions can be made with respect to DA:

- Errors induced by the effective optical depth approach under scattering conditions are often comparable in magnitude to errors caused by uncertainties in ice scattering models, especially for hyperspectral sounders errors, where they can occasionally exceed 0.5 K.
- The more variable gas absorption is within a bandpass, the larger the errors become.
- Especially for hyperspectral sounders for cloud-affected radiance assimilation, it might be possible to choose more spectrally homogeneous regions in which the effect is smaller.
- The more strongly a cloud scatters, the larger the errors become. In the infrared, the single scatter albedo of clouds is around 0.6, which mitigates the issue somewhat. In the visible/near-infrared spectral range the single scatter albedo of clouds is often very close to one and the issue is expected to be worse if, for example, high spectral resolution observations of clouds in near-infrared bands (e.g. GoSat, Orbiting Carbon Observatory (OCO-2)) are to be assimilated using effective optical depth approaches.

A full assessment of this effect under different scattering conditions is an outstanding issue with a potential bearing on further development of gas absorption parametrizations for NWP.

4. The plane-parallel assumption

Under cloudy and precipitating conditions, or, more generally, if spatially highly inhomogeneous fields are observed, the difference between observations and simulations is strongly affected by the inhomogeneity of the observed scene and the inability to accurately simulate the three-dimensional (3D) RT. Simplified methods of allowing for inhomogeneity in models, even advanced cloud overlap parametrizations (such as O'Dell *et al.*, 2007; Geer *et al.*, 2009), are born out of necessity but are by no means capable of simulating or even meant to simulate the actual inhomogeneity observed by the satellite.

Regardless of whether cloud-overlap assumptions are used or if the NWP model is run at a resolution where clouds are resolved explicitly, it is currently inconceivable to use full 3D RT in the context of data assimilation. However, it is still important to understand the errors resulting from our approximations. Here we address the issue for the simple case of a rain cloud for one-dimensional (NWP-like) and slant RT (Bauer *et al.*, 1998; O'Dell *et al.*, 2006) as an approximation to full 3D RT. In order to study the general impact of 3D errors on microwave brightness temperatures we first devised a simplified experiment with a precipitating cloud consisting of just two layers. The lower layer was set to be 3.5 km deep and consisted only of liquid precipitation with a Marshall–Palmer size distribution and 2 g/kg rain water (corresponding to a rain rate of roughly 12 mm/h). A second layer with frozen precipitation was set aloft, the liquid precipitation up to a depth of 11.5 km with an ice mixing ratio of 2 g/kg. The precipitating cloud is assumed to be circular with a radius of 25 km. Water vapour and temperature profiles were used for a tropical atmosphere. An ocean surface with 10 m/s homogeneous wind speed and a surface temperature of 300 K was used. Note that all the above particular values are of relatively minor importance in the framework of this conceptual study.

The satellite zenith angle was set to 55°, a typical value for a conically scanning instrument. The model domain was in total 150×150 km^2 with a horizontal resolution of 1×1 km^2 and a vertical resolution of roughly 500 m. Figure 5 shows the simulation results for one scattering frequency (150 GHz, panels (a)–(d)) and one emission frequency (6.9 GHz, panels (e)–(h)).

The low-frequency emission channel first sees the emission of the side of the cloud reflected off the ocean surface (Position 1 in Figure 5). At this point, differences between the cold ocean surface seen in the plane-parallel case and the reflected cloud in the slant case can be high, exceeding 50 K at 1×1 km^2. Even at the resolution of 50×50 km^2, differences are in the order of -2.5 K with the plane-parallel being colder than the slant model. Reaching Position 2, the satellite basically observes the same brightness temperature both slant and plane-parallel. At Position 3 the plane-parallel model observes the cold ocean background and the slant model still sees cloud emission and is thus warmer.

The negative and positive biases of the plane-parallel model near the cloud edges do not completely cancel out. Overall, the plane-parallel model exhibits a negative bias since the underestimation of the observed brightness temperatures has a stronger effect than the overestimation closer to the cloud edge. This inequity between the magnitude of the positive and negative spikes is caused by

Copyright © 2011 Royal Meteorological Society

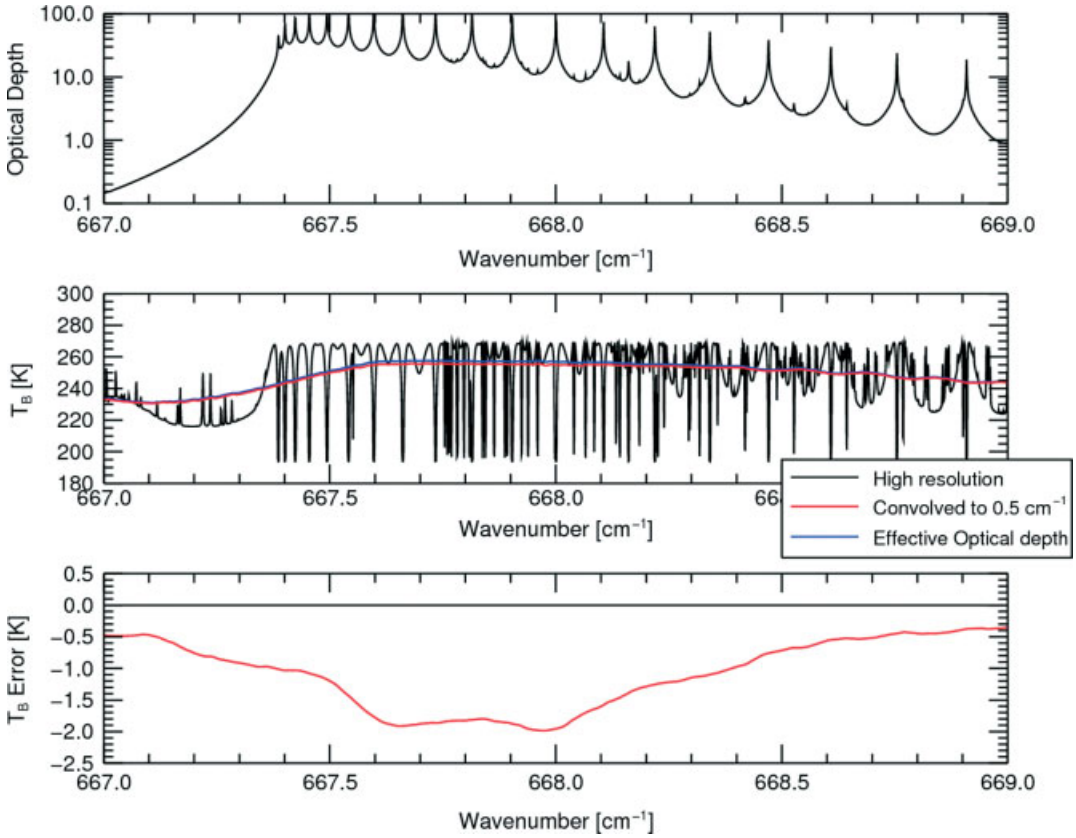

Figure 4. Impact of effective optical depth calculations at high spectral resolution. The upper panel shows the atmospheric nadir optical depth at 0.001 cm^{-1} resolution for a midlatitude standard atmosphere. The mid panel shows the corresponding high-resolution brightness temperatures (black) under the presence of a cirrus cloud of optical depth 1 at 10 km altitude. The red and blue curves (middle panel) show the high-resolution brightness temperatures convolved to 0.5 cm^{-1} (red), and brightness temperatures using effective optical depth calculations at 0.5 cm^{-1} spectral resolution. The lower panel gives the difference between the mid panel's red and blue curves showing the error introduced by the calculations using the effective optical depth.

saturation effects in the observed brightness temperatures. The effect of reflection on brightness temperatures near the left side of the cloud is very effective, since the cloud-free atmosphere basically has near-zero optical depth at 6.9 GHz. Thus differences between plane-parallel and slant are large (exceeding −50 K). The overestimation of brightness temperatures closer to cloud edge in comparison occurs in an optically thicker atmosphere, so the effect is less pronounced (around +40 K). The net effect averaged over a larger area is therefore an underestimation of brightness temperatures for plane-parallel models at emission frequencies. In this particular case the bias over the entire scene of 150 × 150 km^2 is about −1.5 K at horizontal polarization and about −0.8 K at vertical polarization.

The scattering frequency exhibits a different behaviour than the emission frequency. In general the position of the cloud in the slant RT is shifted compared to the position of the plane-parallel cloud. This shift is simply caused by parallax effects caused by the satellite zenith angle and the height of the frozen precipitation above the surface. This effect has been reported before and corrections for this parallax shift, for example in satellite retrievals, have been devised (Bauer *et al.*, 1998). Superimposed over this parallax shift, several other effects are noticed. At Position 1 the slant model produces slightly higher brightness temperatures than the plane-parallel model, caused again by warm emission from liquid precipitation reflections off the ocean surface. At Position 2 the ice starts to affect the brightness temperatures in the slant model and simulated slant brightness temperatures start to decrease until they finally reach the same values as the plane-parallel brightness temperatures. At the right side of the cloud near Position 3 the amount of ice seen by the satellite decreases again and brightness temperatures start to warm again.

At high spatial resolution the differences between the slant and the plane-parallel model can be as large as 120 K. At a lower spatial resolution of 50 × 50 km^2, which is close to the resolution of AMSU-B at zenith angles of around 55°, differences can still be on the order of 10 to 15 K. When averaged over the entire domain, the bias of the plane-parallel RT with respect to slant RT is +1.9 K for vertical polarization and about +2.4 K for horizontal polarization.

These simple considerations highlight several issues associated with forward RT: firstly, the assumption of plane-parallel RT will bias the simulated brightness temperatures. For low frequencies, where emission dominates the signal and by virtue of their low spatial resolution, the biases are comparably small and vary smoothly in space. Such biases can potentially be corrected using an operational bias removal based on comparisons between simulated and observed brightness temperatures. At higher frequencies, where scattering is more pronounced, the overall bias introduced simply by the plane-parallel assumption becomes larger and will become much harder to correct for. In particular, conflicts between quality control and bias removal might become an issue, i.e. if quality control removes observations with biases exceeding a certain value, the bias removal might be adversely affected. In this context,

Copyright © 2011 Royal Meteorological Society

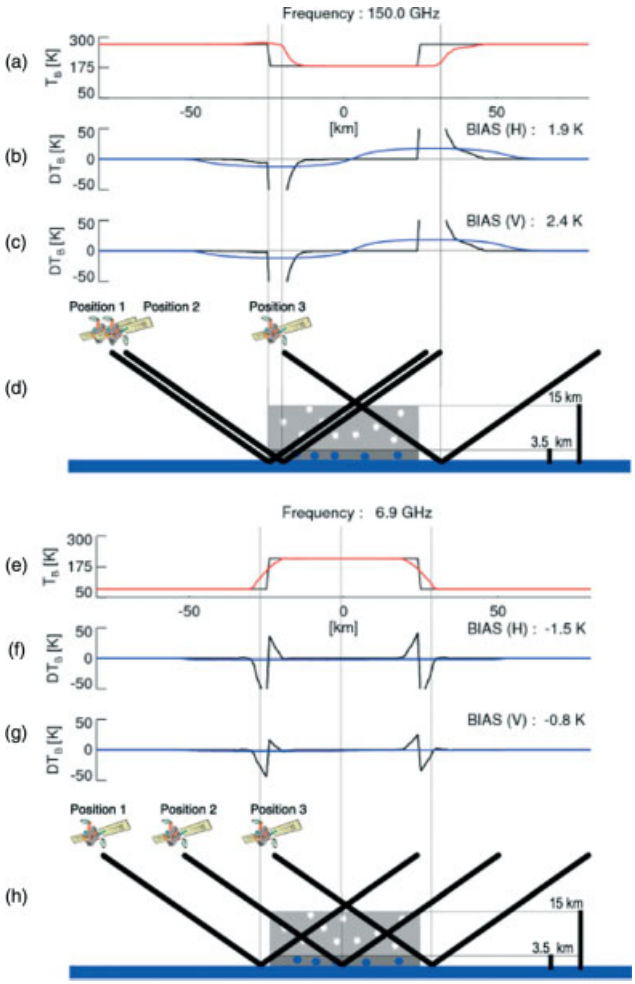

Figure 5. Schematic view of slant path errors due to plane-parallel modelling. The upper panels (a)–(d) show simulated 150.0 GHz brightness temperatures, the lower panels (e)–(h) 6.9 GHz brightness temperatures for a corresponding idealized precipitating cloud over ocean background (for details on the simulation, see text). The black curve in panels (a) and (e) show the simulation results for plane-parallel cases, the red curve for slant geometry. Panels (b), (c), (f) and (g) give the differences between plane-parallel and slant model results for horizontal (b), (f) and vertical (c), (g) polarization. The black curves give the differences at 1×1 km^2 resolution; the blue curves show the same results convolved to 50×50 km^2.

monitoring the bias as a function of cloud liquid water path might help mitigate these issues. Secondly, even when biases are corrected for, large uncertainties will remain (e.g. due to spatial mislocation of features in NWP models). Because of these issues, an averaging of observations over a grid box (rather than data thinning) appears feasible and advantageous for precipitation assimilation in operational DA schemes. The above examples also highlight that biases introduced by the plane-parallel assumption will most likely be correlated among different frequencies, leading to a strong error correlation between different frequencies.

5. Conclusions

This article highlights several current issues related to scattering radiative transfer in data assimilation. While many of these issues have been solved from a mere theoretical standpoint, the inclusion of full scattering radiative transfer into data assimilation remains a challenge because of tight constraints both on accuracy and numerical efficiency. In particular, the following issues were investigated:

(i) Radiative transfer solver errors under scattering conditions: If 2-stream solvers are used, RT solver errors can be on the order of 2–4 K. These errors can be mitigated using 4-stream solvers at the expense of an increase in calculation time by about 60%. A simple 'scattering indicator' is proposed that might help determine beforehand whether or not the use of higher-order solvers is necessary.
(ii) Errors and uncertainties in the parametrization of particle scattering optical properties also yield uncertainties of up to 2–4 K.
(iii) Similarly, the approximation of broad-band channels employing a single radiative transfer calculation using effective optical depths, as done both in RTTOV and CRTM, might also cause errors on the order of 0.5 K under scattering conditions.
(iv) More studies are needed to better understand errors and error correlations in scattering atmospheres caused by the above issues (ii) and (iii).
(v) Errors induced by the general lack of knowledge of three-dimensional cloud structure are discussed as well. At very high spatial resolution, these errors easily exceed 10–20 K. At a spatial resolution of about 50 km, errors are on the order of only a few Kelvin, but still significant.
(vi) Finally, different operational models deal with scattering differently. CRTM treats scattering uniformly for all wavelength regions, i.e. it allows users to use the same solver methodology at all wavelengths. CRTM also allows flexibility in switching between different solvers and streams. In contrast, RTTOV uses disparate but fixed approaches to account for scattering in the microwave and infrared, as well as different cloud overlap schemes and cloud types. The greater flexibility provided by CRTM comes, currently, at the cost of an increased computation time compared to RTTOV.

Some of these issues are easier to overcome than others. Errors introduced by 2-stream radiative transfer solvers can be mitigated using advanced solvers with only a moderate increase in computation cost. From the results presented here, 4-stream solvers appear well suited for most of the microwave and infrared spectral range. Also, the method proposed here to determine the relevance of scattering beforehand might allow one to effectively select an appropriate radiative transfer solver with no computational overhead, ensuring the most efficient solver is used in any given situation.

The interplay of gaseous absorption, scattering, and non-monochromatic bandpasses is another area that has not received much attention over the last few years. A comprehensive study on the accuracy of current operational gas transmittance models under scattering conditions is outstanding. However, errors introduced by scattering should be tolerable in both the infrared and microwave because of the dominance of absorption in the former and the near-monochromatic bandpasses in the latter spectral region. Here too, progress can be made using advanced techniques dealing with gas absorption. These techniques typically use several sub-bands to increase accuracy under arbitrary scattering conditions. While such techniques increase computational cost greatly, especially in the infrared, these issues tie in with the need to simulate

Copyright © 2011 Royal Meteorological Society

spectrally highly resolving infrared instruments such as AIRS and IASI with hundreds or even thousands of channels. A conceivable solution would be to simulate the infrared spectrum at a set of monochromatic wavelengths once and then derive resulting radiances for all infrared instruments by weighting this set of representative wavelengths. While theoretically appealing, it might not be feasible in the near-term, since this approach would require a paradigm shift in the operational software away from simulating separate instruments individually.

Given the stringent demands on computing speed in operational NWP, the errors introduced by neglecting slant as well as true three-dimensional RT cannot be expected to be sufficiently accounted for at any time in the near future. Even if the radiative transfer accounted for such effects, potential mislocations of clouds and precipitation in the NWP model would cause similarly large deviations. These errors can easily be one order of magnitude higher than all other potential error sources potentially rendering observations useless, especially for highly inhomogeneous scenes. As a result, these issues effectively limit the spatial resolution at which cloud and precipitation data can be assimilated. As a reasonable operational compromise, a possible solution could be, for example, to average, rather than thin, microwave observations of clouds and precipitation over a given model grid box. This averaging will likely reduce biases to a level with which DA systems can cope within the operational bias correction framework.

Acknowledgements

The authors would like to thank the editor and two anonymous reviewers for their excellent suggestions. This work was funded by the US Joint Center for Data Assimilation under contract numbers NA10NES4400007 and NA06NES4400002.

Appendix. Symbols

Variable	Symbol	Unit
Planck function	$B = B(\lambda, T) = B_\lambda(T)$	$\frac{\mathrm{W}}{\mathrm{m^2 sr\ \mu m}}$
Radiance	$I = I(\lambda, \theta, \phi) = I_\lambda$	$\frac{\mathrm{W}}{\mathrm{m^2 sr\ \mu m}}$
Zenith Angle	θ	rad
Cosine zenith angle	$\mu = \lvert\cos(\theta)\rvert$	–
Solid Angle	Ω	sr
Volume absorption, scattering, extinction coefficients	$\beta_\mathrm{A}; \beta_\mathrm{S}; \beta_\mathrm{E}$	m^{-1}
Optical depth (w.r.t vertical)	$\tau = \int_z^{\mathrm{TOA}} \beta_\mathrm{E} \mathrm{d}z$	–
Transmission	t	–
Solar constant	$S_\mathrm{S} = S_\mathrm{S}(\lambda)$	$\frac{\mathrm{W}}{\mathrm{m^2\ \mu m}}$
Single scatter albedo	$\omega_0 = \frac{\beta_\mathrm{S}}{\beta_\mathrm{E}}$	–
Asymmetry parameter	g	–
Bandpass filter	$F = F(\lambda)$	–
Scattering indicator	x_s	–

References

Andersson E, Pailleux J, Thépaut J-N, Eyre JR, McNally AP, Kelly GA, Courtier P. 1994. Use of cloud-cleared radiances in three/four-dimensional variational data assimilation. *Q. J. R. Meteorol. Soc.* **120**: 627–653.

Bauer P, Schanz L, Roberti L. 1998. Correction of three-dimensional effects for passive microwave remote sensing of convective clouds. *J. Appl. Meteorol.* **37**: 1619–1632.

Bauer P, Moreau E, Chevallier F, O'Keeffe U. 2006. Multiple-scattering microwave radiative transfer for data assimilation applications. *Q. J. R. Meteorol. Soc.* **132**: 1259–1281.

Baum BA, Heymsfield AJ, Yang P, Bedka ST. 2005. Bulk scattering properties for the remote sensing of ice clouds. Part I: Microphysical data and models. *J. Appl. Meteorol.* **44**: 1885–1895.

Bennartz R, Fischer J. 2000. A modified k-distribution approach applied to narrow band water vapour and oxygen absorption estimates in the near infrared. *J. Quant. Spectrosc. Radiat. Transfer* **66**: 539–553.

Bennartz R, Preusker R. 2006. Representation of the photon pathlength distribution in a cloudy atmosphere using finite elements. *J. Quant. Spectrosc. Radiat. Transfer* **98**: 202–219.

Chen Y, Weng FZ, Han Y, Liu QH. 2008. Validation of the Community Radiative Transfer Model by using CloudSat data. *J. Geophys. Res.* **113**: D00A03, DOI: 10.1029/2007JD009561.

Derber JC, Wu W-S. 1998. The use of TOVS cloud-cleared radiances in the NCEP SSI analysis system. *Mon. Weather Rev.* **126**: 2287–2299.

Errico RM, Ohring G, Bauer P, Ferrier B, Mahfouf J-F, Turk J, Weng FZ. 2007. Assimilation of satellite cloud and precipitation observations in numerical weather prediction models: Introduction to the JAS special collection. *J. Atmos. Sci.* **64**: 3737–3741.

Eyre JR, Woolf HM. 1988. Transmittance of atmospheric gases in the microwave region: A fast model. *Appl. Opt.* **27**: 3244–3249.

Fleming HE, McMillin LM. 1977. Atmospheric transmittance of an absorbing gas. 2: A computationally fast and accurate transmittance model for slant paths at different zenith angles. *Appl. Opt.* **16**: 1366–1370.

Geer AJ, Bauer P, O'Dell CW. 2009. A revised cloud overlap scheme for fast microwave radiative transfer in rain and cloud. *J. Appl. Meteorol. Clim.* **48**: 2257–2270.

Greenwald TJ, Hertenstein R, Vukićević T. 2002. An all-weather observational operator for radiance data assimilation with mesoscale forecast models. *Mon. Weather Rev.* **130**: 1882–1897.

Greenwald TJ, Bennartz R., O'Dell CW, Heidinger AK. 2005. Fast computation of microwave radiances for data assimilation using the 'successive order of scattering' method. *J. Appl. Meteorol.* **44**: 960–966.

Heidinger AK, O'Dell CW, Bennartz R, Greenwald TJ. 2006. The successive-order-of-interaction radiative transfer model. Part I: Model development. *J. Appl. Meteorol. Clim.* **45**: 1388–1402.

Hocking J, Rayer P, Saunders R, Matricardi M, Geer AJ, Brunel P. 2011. *'RTTOV v10 Users Guide.'* EUMETSAT Satellite Application Facility on Numerical Weather Prediction.

Hong G. 2007. Radar backscattering properties of nonspherical ice crystals at 94 GHz. *J. Geophys. Res.* **112**: D22203, DOI: 10.1029/2007JD008839.

Kim M-J. 2006. Single scattering parameters of randomly oriented snow particles at microwave frequencies. *J. Geophys. Res.* **111**: D14201, DOI: 10.1029/2005JD006892.

Kulie MS, Bennartz R, Greenwald TJ, Chen Y, Weng FZ. 2010. Uncertainties in microwave properties of frozen precipitation: Implications for remote sensing and data assimilation. *J. Atmos. Sci.* **67**: 3471–3487.

Kummerow CD. 1993. On the accuracy of the Eddington approximation for radiative transfer in the microwave frequencies. *J. Geophys. Res.* **98**: 2757–2765.

Liu GS. 2004. Approximation of single scattering properties of ice and snow particles for high microwave frequencies. *J. Atmos. Sci.* **61**: 2441–2456.

Liu QH, Ruprecht E. 1996. Radiative transfer model: Matrix operator method. *Appl. Opt.* **35**: 4229–4237.

Liu QH, Weng FZ. 2006. Advanced doubling-adding method for radiative transfer in planetary atmospheres. *J. Atmos. Sci.* **63**: 3459–3465.

Liu X, Smith WL, Zhou DK, Larar A. 2006. Principal component-based radiative transfer model for hyperspectral sensors: Theoretical concept. *Appl. Opt.* **45**: 201–209.

McMillin LM, Fleming HE. 1976. Atmospheric transmittance of an absorbing gas: A computationally fast and accurate transmittance model for absorbing gases with constant mixing ratios in inhomogeneous atmospheres. *Appl. Opt.* **15**: 358–363.

Copyright © 2011 Royal Meteorological Society

Matricardi M. 2005. *'The inclusion of aerosols and clouds in RTIASI, the ECMWF fast radiative transfer model for the infrared atmospheric sounding interferometer*. ' ECMWF Technical Memorandum No. 474.
Matricardi M, Chevallier F, Kelly G, Thépaut J-N. 2004. An improved general fast radiative transfer model for the assimilation of radiance observations. *Q. J. R. Meteorol. Soc.* **130**: 153–173.
Matrosov SY. 2007. Modeling backscatter properties of snowfall at millimeter wavelengths. *J. Atmos. Sci.* **64**: 1727–1736.
Moncet J-L, Uymin G, Lipton AE, Snell HE. 2008. Infrared radiance modeling by optimal spectral sampling. *J. Atmos. Sci.* **65**: 3917–3934.
O'Dell CW, Heidinger AK, Greenwald TJ, Bauer P, Bennartz R. 2006. The successive-order-of-interaction radiative transfer model. Part II: Model performance and applications. *J. Appl. Meteorol. Clim.* **45**: 1403–1413.
O'Dell CW, Bauer P, Bennartz R. 2007. A fast cloud overlap parameterization for microwave radiance assimilation. *J. Atmos. Sci.* **64**: 3896–3909.
Petty GW, Huang W. 2010. Microwave backscatter and extinction by soft ice spheres and complex snow aggregates. *J. Atmos. Sci.* **67**: 769–787.
Rothman LS, Jacquemart D, Barbe A, Benner DC, Birk M, Brown LR, Carleer MR, Chackerian Jr C, Chance K, Coudert LH, Dana V, Devi VM, Flaud J-M, Gamache RR, Goldman A, Hartmann J-M, Jucks KW, Maki AG, Mandin J-Y, Massie ST, Orphal J, Perrin A, Rinsland CP, Smith MAH, Tennyson J, Tolchenov RN, Toth RA, Vander Auwera J, Varanasi P, Wagner G. 2005. The HITRAN 2004 molecular spectroscopic database. *J. Quant. Spectrosc. Radiat. Transfer* **96**: 139–204.
Saunders R, Rayer P, Brunel P, von Engeln A, Bormann N, Strow L, Hannon S, Heilliette S, Liu X, Miskolczi F, Han Y, Masiello G, Moncet J-L, Uymin G, Sherlock V, Turner DS. 2007. A comparison of radiative transfer models for simulating Atmospheric Infrared Sounder (AIRS) radiances. *J. Geophys. Res.* **112**: D01S90, DOI: 10.1029/2006JD007088.
Sherlock V, Collard A, Hannon S, Saunders R. 2003. The Gastropod fast radiative transfer model for advanced infrared sounders and characterization of its errors for radiance assimilation. *J. Appl. Meteorol.* **42**: 1731–1747.
Smith EA, Bauer P, Marzano FS, Kummerow CD, McKague D, Mugnai A, Panegrossi G. 2002. Intercomparison of microwave radiative transfer models for precipitating clouds. *IEEE Trans. Geosci. Remote Sensing* **40**: 541–549.
Weng FZ. 2007. Advances in radiative transfer modeling in support of satellite data assimilation. *J. Atmos. Sci.* **64**: 3799–3807.

Copyright © 2011 Royal Meteorological Society